Materials and Design 56 (2014) 460–467

Contents lists available at ScienceDirect

Materials and Design

journal homepage: www.elsevier.com/locate/matdes

# Gas tungsten arc welding of fine-grained AZ31B magnesium alloys made by powder metallurgy

Jinsun Liao [a,*], Naotsugu Yamamoto [a], Kazuhiro Nakata [b]

[a] Kurimoto Ltd., R&D Dept., 2-8-45 Suminoe, Osaka 559-0021, Japan
[b] JWRI, Osaka University, 11-1 Mihogaoka, Ibaraki, Osaka 567-0047, Japan

ARTICLE INFO

*Article history:*
Received 6 August 2013
Accepted 23 November 2013
Available online 7 December 2013

*Keywords:*
Magnesium
Welding
Porosity
Powder metallurgy
Mechanical property

ABSTRACT

AZ31B magnesium alloys with various grain sizes and oxygen contents were prepared by powder metallurgy (P/M) combined with hot extrusion, and the P/M magnesium alloys were subjected to gas tungsten arc welding (GTAW). Porosities are observed in weld joints of the P/M AZ31B alloys with high oxygen contents. Gas composition analysis of porosity shows that the porosity originates mainly from the decomposition of magnesium hydroxide formed during the fabrication of magnesium alloys. The porosity can be decreased or prevented by reducing the amount of magnesium hydroxide (which is expressed as oxygen content in the present study) in the base materials, through controlling the P/M processing time. Use of a filler rod and/or an insert sheet containing rare earth element La tends to decrease the porosity in weld joints. When oxygen content in P/M AZ31B alloys is reduced to 440 ppm or less, sound weld joints without porosity are obtained. Mechanical test demonstrates that tensile strength of the sound weld joints of P/M AZ31B alloys is at the same level as that of weld joint of a commonly hot-extruded AZ31B alloy.



## 1. Introduction

Magnesium alloys are attractive engineering materials because of their low density and high specific strength. They offer a high potential for use as lightweight structural materials in such transport applications as automobiles and aircraft. Nevertheless, the low toughness and poor room temperature formability of magnesium alloys are limiting their widespread applications [1]. In order to overcome these problems, grain refinement techniques including equal-channel angular processing [2–4], accumulative roll bonding [5] and powder metallurgy (P/M) processes [6–7] have been investigated. Former studies show that P/M process is an effective way to produce magnesium alloys with high strength [6], superior impact toughness [7] and excellent corrosion resistibility [8].

In order to apply the newly developed high-performance P/M magnesium alloys to various kinds of structures, welding or joining technology is indispensable. There have been some studies dealing with the joining of P/M steels, copper alloys and their composites [9–11], but works on the welding of P/M magnesium alloys are rare [12–13]. In general, P/M parts with porous or low density can be joined by solid state joining processes such as friction welding and diffusion bonding, while the P/M parts with high density or minimal porosity may be joined by fusion welding processes such as gas tungsten arc welding and laser welding [14]. Previous works demonstrate that a P/M magnesium alloy can be successfully jointed by friction stir welding [12]; however, weld porosity is formed in laser weld joints of the P/M magnesium alloy even though it has extremely high density [13]. The porosity is argued to result from the expansion of gases that have been entrapped in the base material during the initial production processes and later on are released during welding, although no porosity is observed in the base material by means of microstructural examination [13].

It is well known that magnesium alloys are easily corroded in atmospheric environment, since magnesium is an extremely active metal. The corrosion of magnesium alloys leads to the formation of magnesium hydroxide on the surface of magnesium alloys [15]. Therefore, it is reasonable to suggest that magnesium hydroxide may form on the surface of magnesium alloy powders during P/M process, and magnesium hydroxide is likely entrapped in the final P/M magnesium alloys. The magnesium hydroxide entrapped in the magnesium alloys may lead to porosity formation in fusion welding processes. In the present work, the P/M AZ31B alloys with various magnesium hydroxide amounts, which are measured and expressed as oxygen content in the present work, are produced and subjected to gas tungsten arc welding, aiming to comprehensively understand the formation mechanism of porosity in fusion weld joints of P/M magnesium alloys. The formation mechanism of weld porosity is discussed on the basis of gas composition analysis of porosity. Meanwhile, attempts are made to prevent

* Corresponding author. Tel.: +81 666863259; fax: +81 666863149.
*E-mail address:* j_liao@kurimoto.co.jp (J. Liao).

0261-3069/$ - see front matter © 2013 Elsevier Ltd. All rights reserved.
http://dx.doi.org/10.1016/j.matdes.2013.11.061

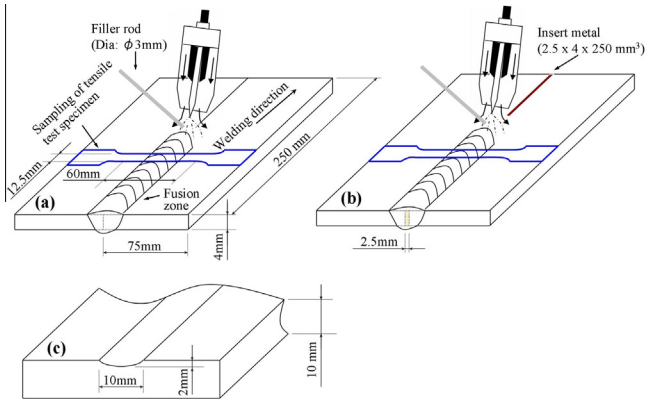


**Fig. 1.** Schematic illustration of gas tungsten arc welding of Mg alloy plates produced by powder metallurgy: (a) butt welding without insert sheet, (b) butt welding with insert sheet and (c) copper backing plate with a groove.

the weld porosity by reducing the oxygen content and using filler rods and/or insert sheets that contain rare earth element La. In addition, the microstructures and mechanical properties of sound weld joints of the P/M AZ31B alloys are also investigated.

## 2. Experimental details

### 2.1. Materials

The materials employed in the present work were AZ31B alloys produced by P/M process combined with hot extrusion. The initial material for the preparation of P/M AZ31B alloys was an ASTM-specified AZ31B cast ingot. Table 1 gives the chemical composition of the AZ31B ingot. The ingot was cut into plates of 210 mm in length, 50 mm in width and 4.5 mm in thickness, and rolled to sheets of 0.7 mm in thickness once by a twin-roller at room temperature, and subsequently crushed to flakes of about 5 mm in diameter by a granulator. The flakes were then collected and pressed again by the twin-roller at room temperature, and the sheets with microcracks, which were formed as a result of pressing the collected flakes, were again crushed to flakes of about 5 mm in diameter by the granulator. The above process was repeated 2–50 times under a controlled atmosphere, so that magnesium flakes produced through above process had various plastic strains and oxygen contents. Subsequently, the flakes were collected and consolidated to billets, and hot-extruded to plates of 75 mm in width and 4 mm in thickness at the extrusion ram speed of 0.5 mm $s^{-1}$ and the extrusion temperature of 623–673 K. Five types of P/M AZ31B plates (marked as sample A, B, C, D and E in the present paper hereafter) having different mean grain sizes in the range of 1.40–2.68 μm and oxygen contents in the range of 140–3500 ppm were produced by changing rolling time of flakes or powders (i.e. powder processing time). For comparison, commonly hot-extruded AZ31B plates (marked as sample F in the present paper hereafter) with extremely low oxygen content were also produced by hot extrusion of billets machined directly from the AZ31B ingot.

### 2.2. Welding parameters

The AZ31B plates including both P/M AZ31B alloys and commonly hot-extruded one were butt welded using gas tungsten arc welding (GTAW) process, as schematically illustrated in Fig. 1. For the purpose of reducing the porosity, butt joints of P/M AZ31B alloys were also designed with an insert sheet of extruded-cast AZXE7113 magnesium alloy (Fig. 1b). Two kinds of filler rods, which were made from extruded-cast AZ61 and AZXE7113 magnesium alloys, were used in the present study. The chemical compositions of AZ61 and AZXE7113 magnesium alloys are given in Table 1, in which the chemical composition of AZ31B base material is also presented. The GTAW parameters are given in Table 2. By the use of the parameters presented in Table 2 and with the help of a copper backing plate, full-penetration single pass weld joints were achieved. The sketch of the copper backing plate is given in Fig. 1c. No back shielding gas was used during welding.

### 2.3. Metallurgical analyses and mechanical test

Before welding, microstructures of P/M AZ31B alloys and commonly hot-extruded one were examined with an optical microscope and transmission electron microscope (TEM, JEOL: JEM-2010), and oxygen content in the AZ31B alloys was analysed with CPAA (Charged Particle Activation Analysis) method, as described in more detail in previous studies [16]. Chemical compositions of magnesium hydroxide and/or oxide particles were analysed with an energy dispersive X-ray (EDX) spectrometer equipped to the TEM. After welding, porosity and microstructures in weld joints were observed by means of an optical microscope and scanning electron microscope (SEM, JEOL: JSM-7000F). An EDX spectrometer equipped to the SEM and X-ray diffractometer (Rigaku: RINT-2000, with a copper target) were employed to ascertain the intermetallic phases in the welds. Specimens for optical microscopy were polished and then etched with a solution of 10 g picric acid, 175 mL ethanol, 25 mL acetic acid, and 25 mL distilled water. Thin foils for TEM observation were prepared by using a focused ion beam instrument and examined with the TEM operated at 160–200 kV.

In addition, gas compositions within the porosity and base metal (BM) of welded specimens were analysed using Anelva AGS-7000 quadruple-pole mass analysis meter, which can measure the gas released from the porosity or BM by drilling the specimens in a vacuum chamber, with the parameters shown in Table 3. The diameter of the drill was 2 mm, and the depth of the drilled conical holes was ca. 3 mm. More information on this analysis is described in Refs. [17–19].

For the sound weld joints, the Vickers hardness profiles of the weld joints were measured on cross sections perpendicular to welding direction. For the hardness measurement, the load was 0.49 N, and dwell time was 20 s. The distance between measurements was 0.5 mm. Tensile specimens with reduced section of 12.5 mm in width, 60 mm in length and 3.8 mm in thickness were machined from the sound weld joint samples as illustrated in Fig. 1, and tensile test was performed according to Japanese Industrial Standards JIS Z 3121 [20] and JIS Z 2241 [21] at room temperature using an Instron servohydraulic load frame operating at a constant crosshead velocity of 1 mm $min^{-1}$. An average of three measurements was used to evaluate the tensile strength of the weld joints.

## 3. Results and discussion

### 3.1. Microstructures and oxygen content in P/M AZ31B alloys

Microstructures of P/M AZ31B alloys (samples A–E) and commonly hot-extruded one (sample F) are shown in Fig. 2, where the mean grain size and oxygen content are given for each sample. All the P/M AZ31B alloys exhibit essentially equiaxed fine grains with mean grain size in the range of 1.40–2.68 μm. The oxygen content in these P/M AZ31B alloys varies from 140 to 3500 ppm, depending on magnesium alloy powder processing time. As the powder processing time is longer, oxygen content in the P/M AZ31B alloy is more. The commonly hot-extruded AZ31B alloy is also essentially equiaxed, but the mean grain size is much larger

**Table 1**
Chemical compositions of magnesium alloys used.

| Magnesium alloy | Chemical composition (mass %) | | | | | | | | | |
|---|---|---|---|---|---|---|---|---|---|---|
| | A1 | Zn | Mn | Si | Fe | Cu | Ni | Be | Ca | La |
| AZ31B alloy | 3.19 | 1.05 | 0.39 | – | 0.003 | 0.010 | 0.0020 | 0.0007 | – | – |
| AZ61 filler rod | 6.25 | 0.98 | 0.29 | 0.01 | 0.001 | 0.001 | 0.0001 | 0.0006 | – | – |
| AZXE7113 filler rod and insert sheet | 6.81 | 0.96 | 0.01 | – | 0.008 | 0.001 | 0.0003 | – | 1.00 | 2.96 |

**Table 2**
Welding parameters.

| Process | Dia. of tungsten electrode | Current | Arc length | Welding speed | Flow rate of Ar shield gas |
|---|---|---|---|---|---|
| GTAW | 3.2 mm | 160–165 A | 1.7 mm | 100 mm/min | 10 ℓ/min |

**Table 3**
Parameters of quadruple-pole mass analysis meter for gas analysis.

| Ionisation energy | 70 eV |
|---|---|
| CEM voltage[a] | −1400 V |
| Mass number range | 2–100 |
| Scanning time | 0.52 s/scan |
| Beginning vacuum degree | about $5 \times 10^{-6}$ Pa |
| Cutting tool | 2$\phi$ drill |

[a] CEM refers to channel electron multiplier.

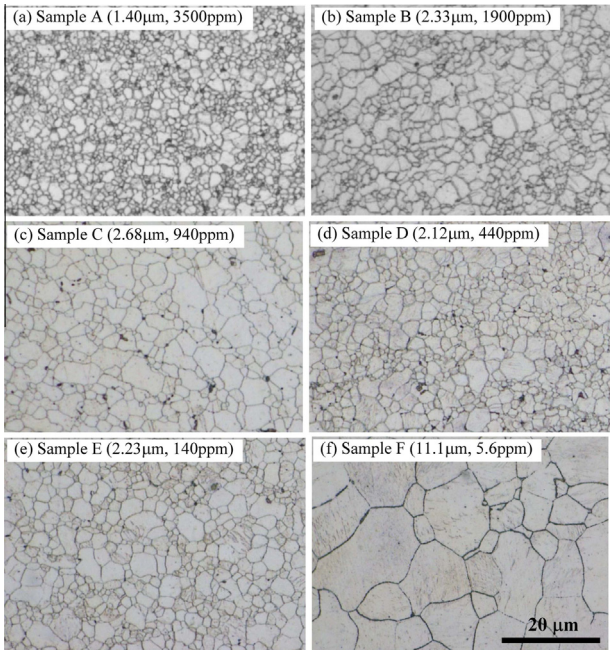


**Fig. 2.** Microstructures of AZ31B alloys with various grain sizes and oxygen contents.

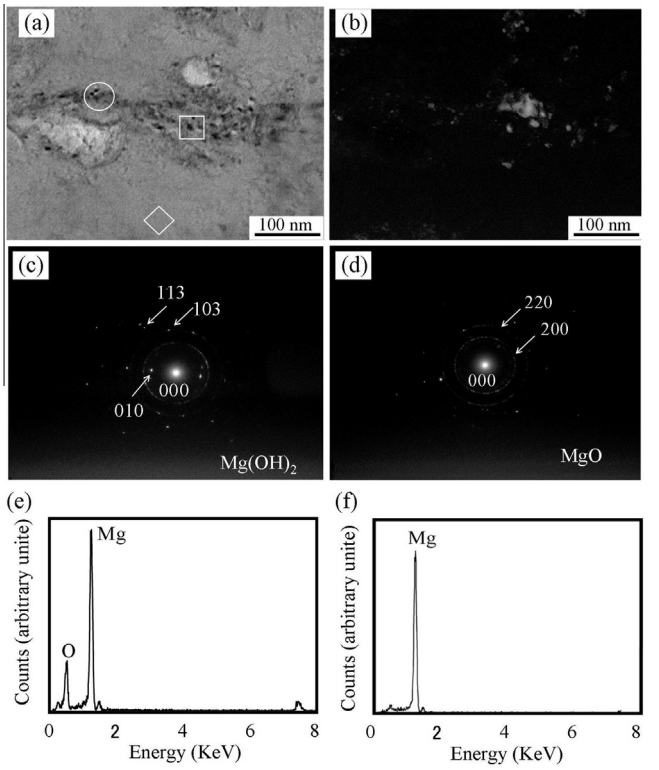


**Fig. 3.** TEM micrographs, electron diffraction patterns and EDX analysis results of magnesium hydroxide and oxide particles in sample B: (a) bright field image, (b) dark field image, (c) electron diffraction pattern of magnesium hydroxide indicated in (a) by a square, (d) electron diffraction rings of magnesium oxide indicated in (a) by a circle, (e) EDX analysis result of magnesium hydroxide particles indicated in (a) by a square, and (f) EDX analysis result of magnesium alloy matrix indicated in (a) by a rhombus.

(11.1 μm) and oxygen content is much less (5.6 ppm). No porosity is observed for all samples.

Fig. 3 reveals TEM micrographs, electron diffraction patterns and EDX analysis results of magnesium hydroxide and oxide particles in sample B, as an example. Magnesium hydroxide and oxide are present in all P/M AZ31B alloys. The magnesium hydroxide and/or oxide particles are in the range of several nanometres to about 30 nm, and exist in the matrix of P/M AZ31B alloys (Fig. 3a and b). Most of the particles are $Mg(OH)_2$ (Hexagonal, $a$ = 0.3144 nm, $c$ = 0.4777 nm) (Fig. 3c), but some of them are MgO (Cubic, $a$ = 0.4211 nm) (Fig. 3d). The magnesium hydroxide is formed as a result of the corrosion of magnesium in the atmosphere where moisture is present [15]. The magnesium hydroxide and/or oxide are also identified by the elemental analysis of the particles and their adjacent matrix (Fig. 3e and f), but they are hardly distinguished from each other only by the elemental analysis because the hydrogen element cannot be detected by the EDX analysis.

It should be noted that the boundaries of AZ31B powders or flakes are hardly observed with optical microscopy and TEM, indicating that most of the powder boundaries have disappeared after hot extrusion, probably because friction and dynamic recrystallisation occurred at the boundaries of powders during hot extrusion [12]. There is no β phase ($Mg_{17}Al_{12}$) in samples A–F, but a few Al–Mn intermetallic particles (dark grey phase in Fig. 2), e.g. $Al_6Mn$

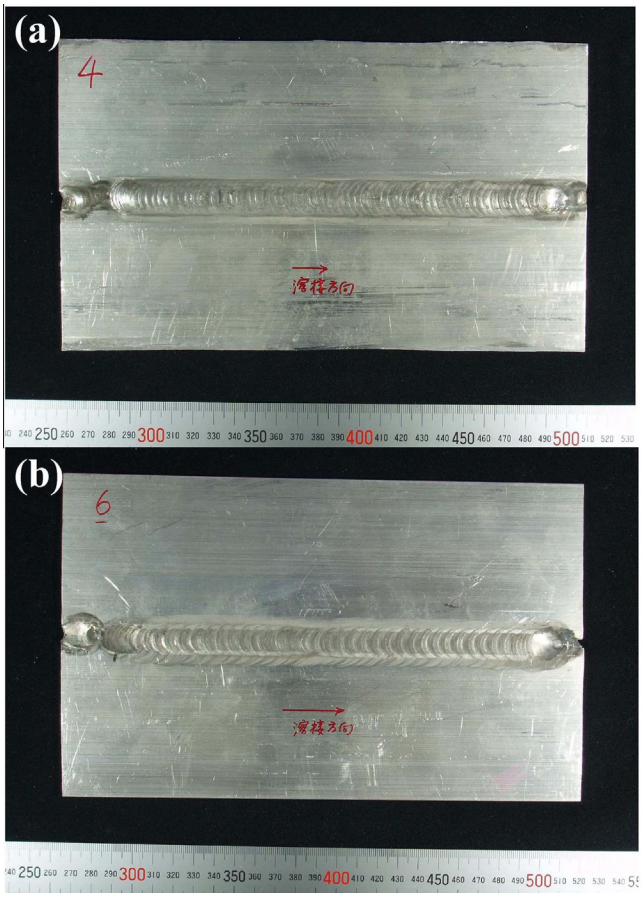


**Fig. 4.** Appearance of GTAW joints of sample B: (a) with AZ61 filler rod but without insert sheet and (b) with both filler rod and insert sheet of AZXE7113..

and/or $Al_8Mn_5$, are present in the interior of grains and at grain boundaries [16]. The P/M AZ31B alloys have comparatively high ultimate tensile strength and yield strength. The yield strength and mean grain size of all samples in the present work are in agreement with the Hall–Petch relationship. Previous works show that the relation between yield strength ($\sigma_y$, unit: MPa) and mean grain size ($d$, unit: μm) can be expressed as $\sigma_y = 150.6 + 115.7\ d^{-1/2}$ [16].

### 3.2. Porosity in welds

The appearance of GTAW joints of sample B is given in Fig. 4, as an example. The GTAW joints of P/M AZ31B alloys exhibit good appearance, and no weld defect is observed from both the front and back surfaces of the joints. However, X-ray radiography reveals that there are enormous volumes of porosity in the GTAW joints of samples A and B, and some porosity in the joint of sample C welded with an AZ61 filler rod, as can be seen from Fig. 5. This is in conformity with the macrostructural examination result of cross-sections of GTAW joints, which are shown in Fig. 6. It is obvious from Fig. 6 that the amount and the size of porosity in the joints of samples A and B are large when they are welded with AZ61 filler rods, and become smaller as AZXE7113 filler rods are used. When both the AZXE7113 filler rods and the insert sheets are used, the amount of porosity in the joints of samples A and B is remarkably decreased. It can also be seen that the amount of porosity is decreased from samples A to C, and almost no porosity is observed in samples D–F. The above results suggest that (i) the use of the filler rod comprising rare earth element La can reduce both the amount and the size of porosity in weld joints, and the use of the insert sheet further diminishes the amount of porosity; (ii) the

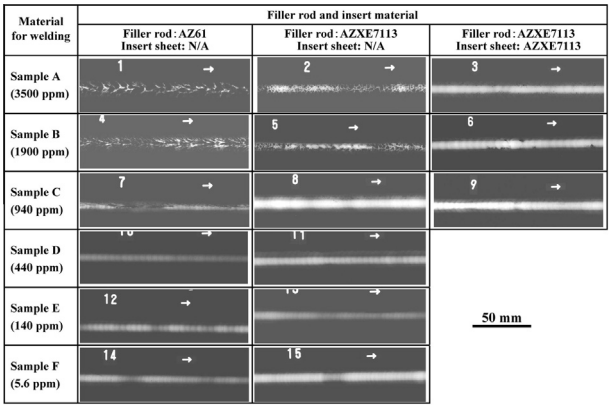


**Fig. 5.** X-ray radiographs of GTAW joints.

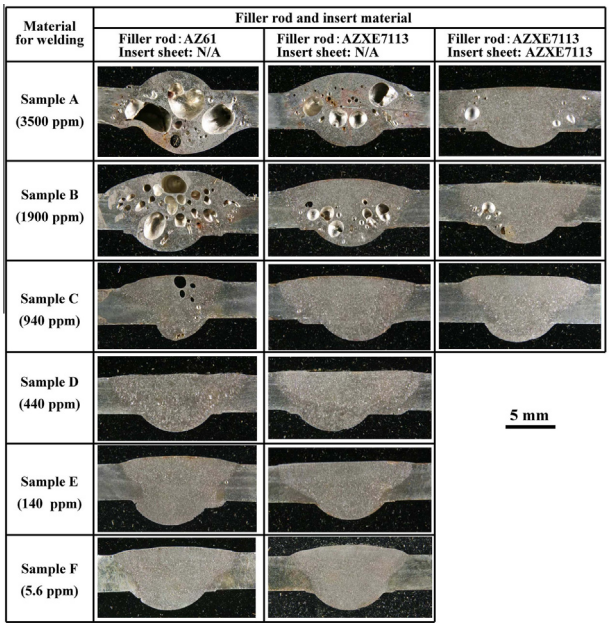


**Fig. 6.** Macrographs of cross-sections of GTAW joints.

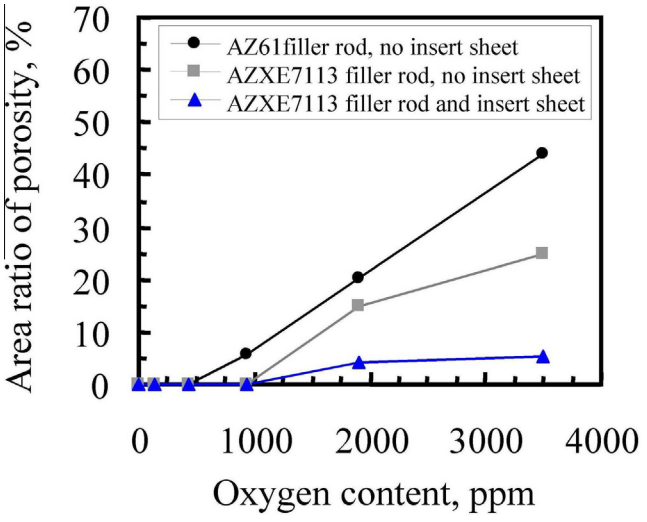


**Fig. 7.** Relation between area ratio of porosity in weld joint and oxygen content in P/M AZ31B alloy.

**Table 4**
Gas composition at different positions in weld joint of sample A welded with AZ61 filler rod but without insert sheet, %.

| Composition | WM 1 | WM 2 | BM |
|---|---|---|---|
| $H_2$ (M/Z[a] 2) | 97.9 | 98.7 | 2.6 |
| $CH_3$ (M/Z[a] 15) | – | – | 19.2 |
| $H_2O$ (M/Z[a] 18) | 1.8 | 1.1 | – |
| $N_2$ (M/Z[a] 28) | 0.3 | 0.2 | 78.2 |
| Total | 100 | 100 | 100 |

[a] M/Z refers to mass number.

porosity in the GTAW joints is depressed when oxygen content in the P/M AZ31B alloys is reduced.

Fig. 7 gives a quantitative relation between oxygen content in the P/M AZ31B alloys and the area ratio of porosity in weld joint. The area ratio of porosity is the proportion of the area of porosity to the area of fusion zone or weld metal (WM), and is calculated according to the photographs of cross-sections of GTAW joints. It is clear from Fig. 7 that the area ratio of porosity is greatly influenced by the oxygen content, the type of filler rod and the insert sheet. The area ratio of porosity decreases with reducing oxygen content in the P/M AZ31B alloys. In the case that the AZ61 filler rod is used, the area ratio of porosity decreases to be nearly zero as oxygen content is 440 ppm or less. In the cases that the AZXE7113 filler rod or both the AZXE7113 filler rod and the insert sheet are used, the area ratio of porosity becomes to be approximately zero as oxygen content is below 940 ppm. The use of the AZXE7113 filler rod significantly reduces the area ratio of porosity in weld joints, as compared to the use of the AZ61 filler rod.

### 3.3. Gas composition in porosity

Gas compositions in porosity and BM of sample A were analysed. The analyses were performed at two different locations in WM and one location in BM. The gas compositions at different positions are shown in Table 4. It can be seen that $H_2$ is the major composition of porosity in WM, whereas the gas in BM consists mainly of $N_2$. Some $CH_3$ is detected in BM, but the origin of $CH_3$ is not understood at present. Considering the accident error of analytical result, there is a possibility that $CH_3$ may be the error of $O_2$ since the M/Z (i.e. the mass number) of $O_2$ is 16, very close to that of $CH_3$. The gas composition analysis result suggests that the gas in BM of the P/M magnesium alloys is formed by air entrapment during P/M process, because the principal composition of the gas in the BM is $N_2$, which is the main composition of air. A little $H_2$ is also found in BM. $N_2$ and $O_2$ in BM originate from air, whereas $H_2$ in BM probably comes from the reaction of Mg and moisture on the surface of Mg alloy plates. The formation of $H_2$, which is developed by the reaction between Mg and $H_2O$, is discussed in detail in the following section. The $H_2$ developed by the reaction may diffuse into metals [22], and this is probably the reason that $H_2$ is detected in BM of magnesium alloys. The existence of $H_2$ in BM of magnesium alloy is also reported elsewhere [19]. It can also been seen from Table 4 that $N_2$ inside porosity in WM is scarce although it is the major component of the gas in BM. This is probably because the gas inside porosity comes mainly from the decomposition of magnesium hydroxides, as described in detail in the following section, and the ratio of $N_2$ from BM is too low inside porosity. It should be noted that gas volume in BM is extremely small as compared to that in WM.

### 3.4. Porosity formation mechanism and its prevention in welds of P/M magnesium alloys

It has been documented that porosity formation in weld joints of magnesium alloys is attributed to (i) hydrogen rejection from the solid phase during solidification [23–24], and/or (ii) coalescence and expansion of small preexisting pores or gas inclusions in BM due to heating and reduction in internal pressure [13,19,25–26], and/or (iii) entrapment of shielding gas induced by turbulent flow in the weld pool or imperfect collapse of the keyhole during laser welding [19,26]. The gas composition in the porosity formed by hydrogen rejection is $H_2$, while that in the porosity due to coalescence and expansion of small preexisting pores or entrapment of shielding gas consists mainly of $N_2$ or shielding gas composition, respectively. Since $H_2$ is the principal composition of porosity in the present work (Table 4), hydrogen rejection seems to be the mechanism for the porosity formation. However, the porosity formed due to hydrogen rejection is usually small [27], dissimilar to the porosity with large sizes in the present work, and in particular the conventional hydrogen rejection mechanism cannot explain the phenomenon that the area ratio of porosity in weld joint is various for different P/M AZ31B alloys (Figs. 6 and 7). Because magnesium alloys are likely corroded in atmospheric environment and magnesium hydroxide is formed on the surface of magnesium alloy powders [15–16,27], the porosity formation mechanism in weld joints of P/M magnesium alloys can be proposed as follows.

As demonstrated by TEM observation together with electron diffraction and EDX analysis, magnesium hydroxide exists in the P/M AZ31B alloys. The magnesium hydroxide is produced on the magnesium alloy powder surface due to atmospheric corrosion of magnesium alloys. The atmospheric corrosion of magnesium alloys can be expressed by the following reactions [1527]:

$$Mg \rightarrow Mg^{2+} + 2e^{-} \text{(anodic reaction)} \quad (1)$$

$$2H_2O + 2e^{-} \rightarrow H_2 + 2OH^{-} \text{(cathodic reaction)} \quad (2)$$

$$O_2 + 2H_2O + 4e^{-} \rightarrow 4OH^{-} \text{(cathodic reaction)} \quad (3)$$

$$Mg^{2+} + 2OH^{-} \rightarrow Mg(OH)_2 \text{ (product formation)} \quad (4)$$

The $H_2O$ needed for the corrosion reaction comes from the humidity or moisture in atmosphere, and the corrosion reaction can occur at room temperature. The corrosion product $Mg(OH)_2$ on the surface of magnesium alloy powders, which exists as thin film or particles, will be entrapped into powder billets and included in magnesium alloys finally produced by hot-extrusion. With the increase in magnesium alloy powder processing time, more magnesium hydroxide particles or films are included in P/M AZ31B alloys. This is the reason why the oxygen content is increased from samples E to A (Fig. 2).

When the P/M AZ31B alloys are welded by GTAW process, the magnesium alloys are melted at fusion zone, and the magnesium hydroxide is decomposed into magnesium oxide (MgO), oxygen and hydrogen gases, as expressed by the following reactions:

$$Mg(OH)_2 \rightarrow MgO + H_2O \quad (5)$$

$$2H_2O \rightarrow 2H_2 + O_2 \quad (6)$$

Oxygen will react with magnesium to form magnesium oxide at high temperature, and the magnesium oxide formed by both magnesium hydroxide decomposition and reaction of magnesium with oxygen will float onto the surface of weld pool. Hydrogen may react with magnesium to form the magnesium hydride ($MgH_2$) at high pressure and high temperature with the help of catalysts [28], but this reaction is extremely difficult without catalysts. Hydrogen can dissolve into the molten magnesium alloy to some extent, as indicated by the binary alloy phase diagram of hydrogen and magnesium [29], but hydrogen may remain in weld pool to form porosity in weld joints after solidification if the amount of

hydrogen exceeds the solution limit. In addition, the hydrogen dissolved in molten magnesium alloy will be rejected from the liquid to solid magnesium during solidification to form porosity (i.e. the hydrogen rejection mechanism), because of the difference in solubility between liquid and solid magnesium.

The above mechanism can explain the phenomena observed in the present study. The hydrogen in the porosity comes from the decomposition of magnesium hydroxide formed during manufacturing process of P/M AZ31B alloys. With the decrease in the amount of magnesium hydroxide, which is expressed as oxygen content in the present study, the hydrogen produced from decomposition of magnesium hydroxide becomes less, so that the area ratio of porosity in weld joints is reduced (Fig. 7). When oxygen content is 440 ppm or less, there is almost no porosity in weld joints (Figs. 6 and 7). This is probably because the amount of hydrogen produced in the weld pool is small, and the hydrogen has completely dissolved into magnesium alloy matrix after solidification or escaped from the weld pool before solidification.

It is also interesting to note that there is a little of $H_2O$ and $N_2$ in porosity in WM (Table 4). The existence of $H_2O$ in porosity supports the mechanism proposed above. According the mechanism described above, the $H_2O$ comes from the decomposition of magnesium hydroxide Eq. (5). It is because the $H_2O$ is not completely decomposed during welding, a little of $H_2O$ is remained and detected in the porosity. The $N_2$ in porosity in WM originates from the entrapped gas in BM. Therefore, the mechanism of coalescence and expansion of gas inclusions may, in part, contribute to the formation of porosity.

As shown in Fig. 6, porosity in weld joints is generally of large size, and most of the pores exhibit globular shape or elongated globular shape, but some of them have irregular shapes. These irregular pores are probably formed by the coalescence of two or more globular pores. A few of the pores are located close to the fusion line or connected to the fusion line via a narrow channel. These characteristics of morphology and distribution of porosity in WM are similar to those of the porosity formed by the coalescence and expansion of small preexisting pores or entrapped gas in BM reported in previous works [13,19]; however, most of pores in WM are not formed by the coalescence and expansion of small preexisting pores or entrapped gas in BM in the present work, because the gas composition inside porosity is principally $H_2$, different from that inside the porosity formed by the coalescence and expansion of entrapped gas in BM, which consists mainly of $N_2$. The porosity is formed predominantly due to the decomposition of magnesium hydroxide and consequent evolution of $H_2$, and these pores may expand to become large in size at high temperature, resulting in a similar morphology to those formed by the coalescence and expansion of entrapped gas in BM. Of course, the gas in BM may also contribute to the formation of porosity in WM by coalescence and expansion. From both the morphology and gas composition of porosity, it can be suggested that magnesium hydroxide decomposition is the principal porosity formation mechanism, and the coalescence and expansion of entrapped gas in BM may also be partly responsible for the porosity formation in WM in the present work.

In the previous work [13], AZ31B magnesium alloy produced by rapid solidification powder metallurgy, a different P/M process from that used in the present work, was subjected to laser welding. Many large pores were formed in WM. This phenomenon is similar to that observed in the present work. It was reported that porosity in WM of the laser weld joint originated from BM and was formed by coalescence and expansion of entrapped gas during welding, and magnesium oxide particles were found inside porosity. The major mechanism of porosity formation in the previous work is different from that in the present work, probably because P/M process is different and magnesium hydroxides are less or not included in the AZ31B alloy in the previous work. Another reason is probably that the gas inclusion in BM is more in the previous work than in the present work. Since the solidification speed of laser welding is extremely high, the magnesium oxides are likely entrapped inside the porosity in the previous work. In contrast, the solidification speed of gas tungsten arc welding is low, thus magnesium oxides have enough time to float onto the surface of weld pool in the present work.

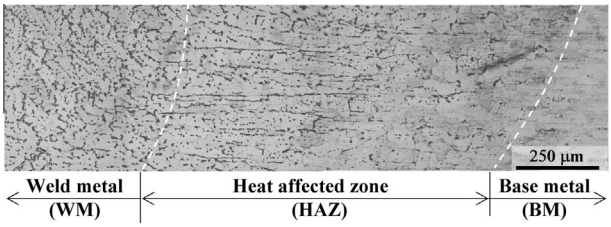


**Fig. 8.** Microstructures at weld joint of sample D welded with an AZXE7113 filler rod but no insert sheet.

It can be seen from Figs. 6 and 7 that the use of AZXE7113 filler rods containing rare earth element La has depressed the formation of porosity. The effect of La on the suppression of porosity is also reported in other studies [19,30]. It is suggested that rare earth element La can absorb hydrogen or react with hydrogen to form hydrides at high temperatures, thus free hydrogen content in liquid alloy is reduced, and the amount of porosity is decreased [31]. The use of both AZXE7113 filler rods and insert sheets further decreases the formation of porosity in weld joints, because the portion of P/M magnesium alloy to be melted in weld pool becomes less due to the use of an insert sheet, leading to the decrease in porosity in weld joints.

In summary, in order to prevent the porosity in weld joints of P/M AZ31B alloys, it is necessary to reduce the amount of magnesium hydroxide in the BM. Use of filler rods containing rare earth element La and/or of insert sheets is beneficial to reduce porosity in weld joints of P/M magnesium alloys.

### 3.5. Microstructures and mechanical property of sound weld joints

It can be seen from Fig. 6 that sound weld joints without porosity are achieved when oxygen content in P/M AZ31B alloys (e.g. in samples D and E) is 440 ppm or less. In this section, the microstructures and mechanical properties of the sound weld joints of samples D and E are investigated in detail and compared to those of commonly hot-extruded AZ31B alloy (i.e. sample F).

Fig. 8 shows microstructures across the weld joint of sample D, as an example. WM is characterised as equiaxed magnesium grains and second phases. No porosity is observed in the WM and its adjacent heat affected zone (HAZ). HAZ consists of two parts. At the HAZ adjacent to WM, lath-like structure is observed probably because the original boundaries of magnesium alloy powders or flakes, whose cross-section is lath-like before hot-extrusion, are partly melted during welding. At the HAZ adjacent to BM, the grains become much coarser as compared to those in BM.

Detailed microstructures in the WMs of sample E welded by using the AZ61 filler rod and AZXE7113 filler rod are given in Fig. 9a and b, respectively. Many second phase particles are present in the WMs. The second phase in the WM produced by the use of the AZ61 filler rod is β phase ($Mg_{17}Al_{12}$). The second phases in the WM produced by the use of the AZXE7113 filler rod include mainly $Al_4Ca$, $Al_{11}La_3$ and $Al_3La$, as indicated by the XRD analysis result shown in Fig. 10. Elemental mapping analyses using the EDX attached to SEM reveal that grainy particles at grain

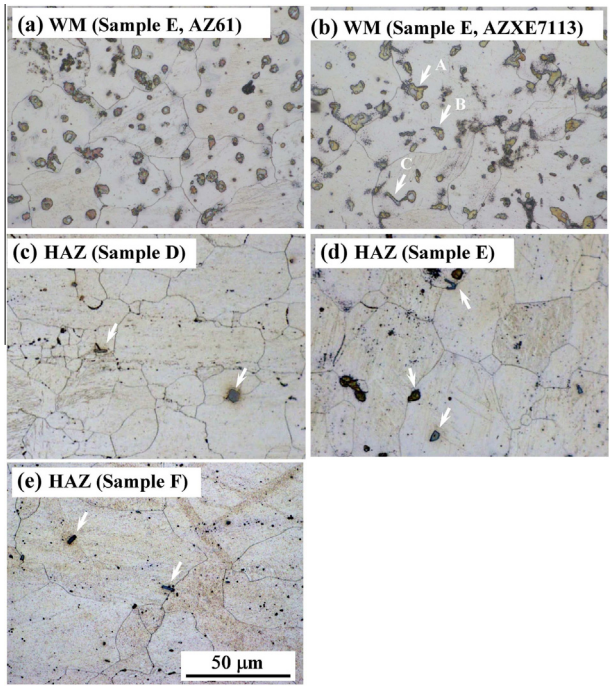


**Fig. 9.** Microstructures at various zones of weld joints.

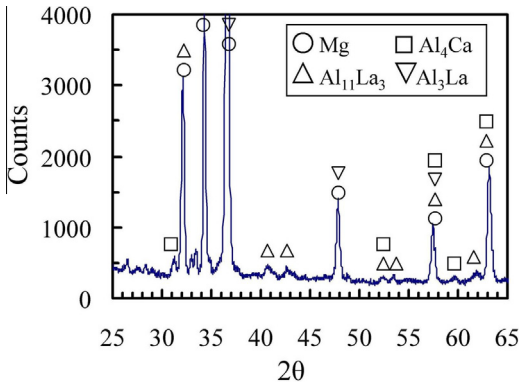


**Fig. 10.** XRD patterns of weld metal of sample E welded with an AZXE7113 filler rod.

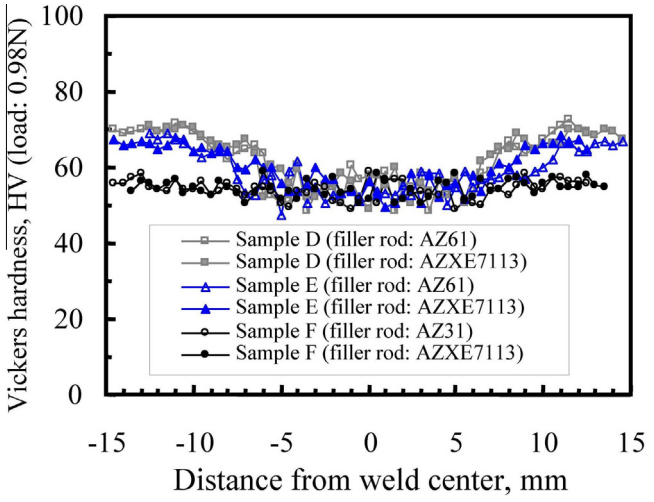


**Fig. 11.** Hardness distribution across the weld joints of samples D–F.

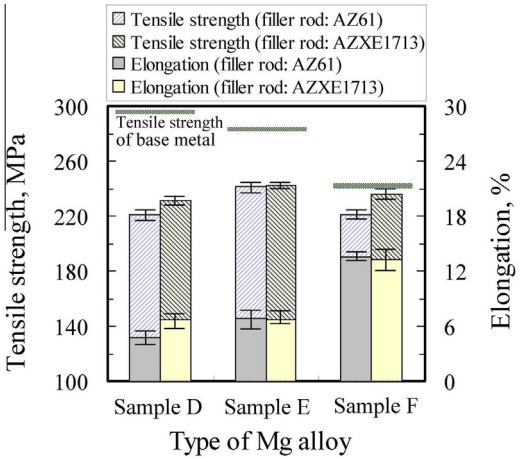


**Fig. 12.** Tensile test result of weld joints of samples D–F.

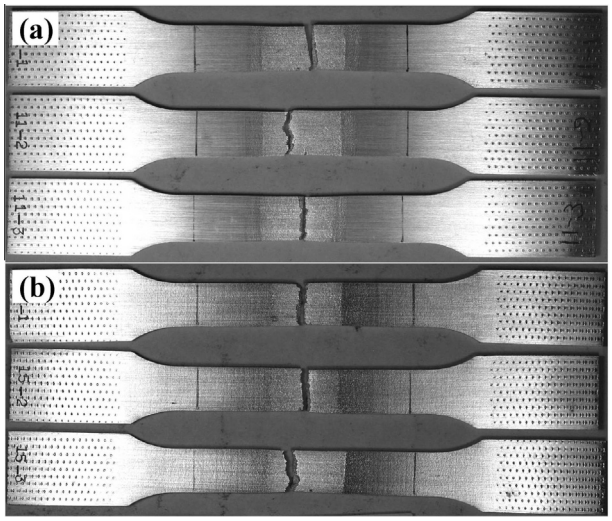


**Fig. 13.** Appearance of tensile tested specimens: (a) sample D welded with AZXE7113 filler rod but no insert sheet and (b) sample F welded with AZXE7113 filler rod but no insert sheet.

boundaries (indicated by arrow A in Fig. 9b) are principally $Al_4Ca$ and partly $Al_2Ca$, while grainy particles within the grains (indicated by arrow B in Fig. 9b) are $Al_3La$, and the rod-like particles within grains (indicated by arrow C in Fig. 9b) are $Al_{11}La_3$. As shown in Fig. 9c–e, microstructures at HAZs of samples D, E and F are similar. The grains in these HAZs are coarsened as compared to those in the BMs, and a few of Al–Mn intermetallic particles (grey dark particles in Fig. 9c–e) are observed. Among these HAZs, the grain size in the HAZ of sample D seems to be the smallest and that in the HAZ of sample F is the largest. It should be noted that the microstructures in the WMs of samples D–F are nearly identical provided that the same type of filler rod is used, because welding parameters are the same. The original microstructures of BMs have little influence on the microstructures in WMs. When different type of filler rod is used, the microstructures in the WMs are different, as shown in Fig. 9a and b.

Fig. 11 gives the hardness profiles across weld joints of samples D–E. The hardness in the WMs of samples D–E is at the same level, but the hardness in the HAZs or BMs is different for the three samples. The hardness in the HAZ or BM of sample D is the highest, while that of sample F is the lowest. It can be seen that the

hardness in the BM and HAZ is higher than that in the WM for samples D and E, but the hardness in the BM, HAZ and WM is approximately identical for sample F.

The tensile test results of weld joints of samples D–F are shown in Fig. 12, where the tensile strength of BM of samples D–F is also presented for reference. The tensile strength of weld joints of samples D–F is at the same level. As shown in Fig. 13 by the way of example, all the tensile test specimens are broken at WMs whose hardness is almost the same for these samples. The elongation of weld joint of sample F is much higher than that of samples D and E. This is because the hardness at the WM, HAZ and BM of sample F is close, and deformation can occur at whole specimen during tensile test. In contrast, the deformation concentrates on WM due to its lowest hardness in the joints for samples D and E.

## 4. Conclusions

Gas tungsten arc welding was applied to AZ31B magnesium alloys produced by powder metallurgy combined with hot extrusion. The porosity formation behaviour in weld joints was observed, and the porosity formation mechanism was discussed on the basis of gas composition analysis of porosity. Besides, the microstructures and mechanical properties of sound weld joints of P/M AZ31B alloys were investigated and compared to those of commonly hot-extruded AZ31B alloy. The results can be summarised as follows.

(1) Porosity is observed in weld joints of the P/M AZ31B alloys with high oxygen contents, but not found in weld joints of the P/M AZ31B alloys with low oxygen contents (e.g. 440 ppm or less). The porosity in weld joints of P/M AZ31B alloys can be prevented by reducing oxygen content in the alloys. Use of a filler rod containing La element tends to reduce the porosity in weld joints. Combinational use of a filler rod and insert sheet further depresses porosity formation.
(2) The porosity in weld joints of P/M AZ31B alloys results mainly from the decomposition of magnesium hydroxide ($Mg(OH)_2$) which forms on the surface of AZ31B alloy powders during P/M process and is entrapped into the P/M AZ31B alloys during billet preparation and hot extrusion. The magnesium hydroxide is decomposed during arc welding and thus hydrogen gas is developed in weld pool, leading to porosity formation in weld metals. This mechanism can explain the phenomenon that the porosity is observed in weld joints of P/M AZ31B alloys with high oxygen contents but not in weld joints of P/M AZ31B alloys with low oxygen contents.
(3) Sound weld joints without any defect are achieved for the P/M AZ31B alloys whose oxygen content is 440 ppm or less. The tensile strength of weld joint of P/M AZ31B alloys is at the same level as that of commonly hot-extruded one, but the elongation of weld joint is lower as compared to the commonly hot-extruded AZ31B alloy, because the deformation during tensile test concentrates on the weld metal for the P/M AZ31B alloys.

## References


[1] Agnew SR, Yoo MH, Tome CN. Application of texture simulation to understanding mechanical behavior of Mg and solid solution alloys containing Li or Y. Acta Mater 2001;49:4277–89.
[2] Suwas S, Gottstein G, Kumar R. Evolution of crystallographic texture during equal channel angular extrusion (ECAE) and its effects on secondary processing of magnesium. Mater Sci Eng A 2007;471:1–14.
[3] Chuvil'deev VN, Nieh TG, Yu Gryaznov M, Sysoev AN, Kopylov VI. Low-temperature superplasticity and internal friction in microcrystalline Mg alloys processed by ECAP. Scripta Mater 2004;50:861–5.
[4] Ma A, Jiang J, Saito N, Shigematsu I, Yuan Y, Yang D, Nishida Y. Improving both strength and ductility of a Mg alloy through a large number of ECAP passes. Mater Sci Eng A 2009;513–514:122–7.
[5] del Valle JA, Pérez-Prado MT, Ruano OA. Accumulative roll bonding of a Mg-based AZ61 alloy. Mater Sci Eng A 2005;410–411:353–7.
[6] Elsayed A, Umeda J, Kondoh K. Application of rapid solidification powder metallurgy to the fabrication of high-strength, high-ductility Mg–Al–Zn–Ca–La alloy through hot extrusion. Acta Mater 2011;59:273–82.
[7] Liao J, Hotta M, Kaneko K, Kondoh K. Enhanced impact toughness of magnesium alloy by grain refinement. Scripta Mater 2009;61:208–11.
[8] Liao J, Hotta M, Mori Y. Improved corrosion resistance of a high-strength Mg–Al–Mn–Ca magnesium alloy made by rapid solidification powder metallurgy. Mater Sci Eng A 2012;544:10–20.
[9] Jayabharath K, Ashfaq M, Venugopal P, Achar DRG. Investigations on the continuous drive friction welding of sintered powder metallurgical (P/M) steel and wrought copper parts. Mater Sci Eng A 2007;454–455:114–23.
[10] Fillabi MG, Simchi A, Kokabi AH. Effect of iron particle size on the diffusion bonding of Fe–5%Cu powder compact to wrought carbon steels. Mater Des 2008;29:411–7.
[11] Suresh MV, Vamsi Krishna B, Venugopal P, Prasad Rao K. Effect of pulse frequency in gas tungsten arc welding of powder metallurgical preforms. Sci Technol Weld Join 2004;9:362–8.
[12] Liao J, Yamamoto N, Nakata K. Effect of Dispersed Intermetallic Particles on Microstructural Evolution in the Friction Stir Weld of a Fine-Grained Magnesium Alloy. Metall Mater Trans A 2009;40:2212–9.
[13] Wahba M, Kawahito Y, Kondoh K, Katayama S. A fundamental study of laser welding of hot extruded powder metallurgy (P/M) AZ31B magnesium alloy. Mater Sci Eng A 2011;529:143–50.
[14] Selcuk C, Bond S, Woollin P. Joining processes for powder metallurgy parts: a review. Powder Metall 2010;53:7–11.
[15] Liao J, Hotta M, Motoda S, Shinohara T. Atmospheric corrosion of two field-exposed AZ31B magnesium alloys with different grain size. Corros Sci 2013;71:53–61.
[16] Liao J, Hotta M, Koshi A. Effect of oxygen content on impact toughness of a fine-grained magnesium alloy. Mater Lett 2011;65:2995–9.
[17] Ono A, Hayakawa Y, Ueki K, Okayama J, Ban K. Calibration Method for Determination of Nitrogen Content in Steel by Thermo-Conductimetry after Fusion in the Current of an Inert Gas. Anal Sci 1994;10:393–8.
[18] Murakami T, Nakata K, Ikeda T, Nakajima H, Ushio M. Weld fusion property of lotus-type porous copper by laser beam irradiation. Mater Sci Eng A 2003;357:134–40.
[19] Yu L, Nakata K, Liao J. Weld porosity in fibre laser weld of thixomolded heat resistant Mg alloys. Sci Technol Weld Join 2009;14:554–8.
[20] JIS Z 3121: Methods of tensile test for butt welded joints. Japanese Standards Association; 2005.
[21] JIS Z 2241: Method of tensile test for metallic material. Japanese Standards Association; 2005.
[22] Tsuru T, Huang Y, Ali MdR, Nishikata A. Hydrogen entry into steel during atmospheric corrosion. Corros Sci 2005;47:2431–40.
[23] Mikucki BA, ShearouseIII JD, Proceedings of magnesium properties and applications for automobiles conference. Detroit (Mich.): Society of Automotive Engineers, Inc.; 1993. p. 107–15.
[24] Liu L, Song G, Liang G, Wang J. Pore formation during hybrid laser-tungsten inert gas arc welding of magnesium alloy AZ31B—mechanism and remedycle. Mater Sci Eng A 2005;390:76.
[25] Haferkamp H, Bach Fr-W, Burmester I, Kreutzburg K, Niemeyer M. In: Proceedings of the third international magnesium conference. London (UK): The Institute of Materials; 1996. p. 89–98.
[26] Zhao H, Debroy T. Pore Formation during Laser Beam Welding of Die-Cast Magnesium Alloy AM60B - Mechanism and Remedy. Weld J 2001;80: 204s–10s.
[27] Jönsson M, Persson D, Thierry D. Corrosion product formation during NaCl induced atmospheric corrosion of magnesium alloy AZ91D. Corros Sci 2007;49:1540–58.
[28] Zuckerman JJ. Inorganic Reactions and Methods (Vol.2) —The Formation of the Bond to Hydrogen (Part 2). VILEY-VCH publishers, Inc; 1987.
[29] Massalski TB. Binary alloy phase diagrams. Materials Park (OH): ASM International; 1986. p. 2033–6.
[30] Lu Y, Wang Q, Zeng X, Ding W, Zhai C, Zhu Y. Effects of rare earths on the microstructure, properties and fracture behavior of Mg–Al alloys. Mater Sci Eng A 2000;278:66–76.
[31] Li D, He Z, Zhao Y, Wang S, Liou Z. Effect of Rare Earth Elements on the formation of Gas Blowholes in Cast Aluminum Alloy. J Chinese Rare Earth Soc 1987;5(4):39–46.